NANO · MICRO small
www.small-journal.com

# Optimization of Mixed Micelles Based on Oppositely Charged Block Copolymers by Machine Learning for Application in Gene Delivery

*Katharina Leer, Liên S. Reichel, Julian Kimmig, Friederike Richter, Stephanie Hoeppener, Johannes C. Brendel, Stefan Zechel, Ulrich S. Schubert,* and Anja Traeger**

**The COVID-19 mRNA vaccines represent a milestone in developing non-viral gene carriers, and their success highlights the crucial need for continued research in this field to address further challenges. Polymer-based delivery systems are particularly promising due to their versatile chemical structure and convenient adaptability, but struggle with the toxicity-efficiency dilemma. Introducing anionic, hydrophilic, or "stealth" functionalities represents a promising approach to overcome this dilemma in gene delivery. Here, two sets of diblock terpolymers are created comprising hydrophobic poly(*n*-butyl acrylate) (P*n*BA), a copolymer segment made of hydrophilic 4-acryloylmorpholine (NAM), and either the cationic 3-guanidinopropyl acrylamide (GPAm) or the 2-carboxyethyl acrylamide (CEAm), which is negatively charged at neutral conditions. These oppositely charged sets of diblocks are co-assembled in different ratios to form mixed micelles. Since this experimental design enables countless mixing possibilities, a machine learning approach is applied to identify an optimal GPAm/CEAm ratio for achieving high transfection efficiency and cell viability with little resource expenses. After two runs, an optimal ratio to overcome the toxicity-efficiency dilemma is identified. The results highlight the remarkable potential of integrating machine learning into polymer chemistry to effectively tackle the enormous number of conceivable combinations for identifying novel and powerful gene transporters.**

## 1. Introduction

In recent decades, research on non-viral gene carriers has advanced tremendously creating safe and effective vaccines based on lipid nanoparticles.[1,2] However, the limited success of this technology for more complex applications underscores the urgent need for stable delivery systems to effectively address future gene delivery challenges. Efficient delivery systems for genetic material have to meet a range of requirements: i) Stable packaging, ii) protection, iii) safe transport of the genetic payload, iv) high efficiency, and v) a safe profile.[3] Besides lipid-based delivery systems, cationic polymers represent a promising material class, offering the advantage of chemical variety and synthetic versatility with defined structure and composition.[4–7] In particular, amphiphilic block copolymers have gained attention as delivery systems in biomedicine due to the increased stability and efficiency.[8–11] Amphiphilic block copolymers containing a hydrophobic and a hydrophilic segment can self-assemble into core-shell micelles.[12,13]

K. Leer, L. S. Reichel, J. Kimmig, F. Richter[+], S. Hoeppener, J. C. Brendel, S. Zechel, U. S. Schubert, A. Traeger
Laboratory of Organic and Macromolecular Chemistry
Friedrich Schiller University Jena
Humboldtstrasse 10, 07743 Jena, Germany
E-mail: Ulrich.Schubert@uni-jena.de; anja.traeger@uni-jena.de

J. Kimmig, S. Hoeppener, J. C. Brendel, S. Zechel, U. S. Schubert, A. Traeger
Jena Center for Soft Matter (JCSM)
Friedrich Schiller University Jena
Philosophenweg 7, 07743 Jena, Germany

The ORCID identification number(s) for the author(s) of this article can be found under https://doi.org/10.1002/smll.202306116

[+]Present address: NGP Polymers GmbH, Botzstrasse 5, 07743 Jena, Germany



**DOI: 10.1002/smll.202306116**

For gene delivery, cationic charges are integrated into the shell to form so-called micelleplexes improving cellular uptake and endocytosis.[14–16] However, cationic micelles are also known to induce cytotoxic effects due to their cationic surface charge density.[17] Incorporating a "stealth" polymer, such as poly(ethylene glycol) (PEG, or poly(ethylene oxide) (PEO)), can mitigate cytotoxicity, reduces binding to serum proteins, and results in extended blood circulation time.[18,19] However, this positive effect of PEGylation is accompanied by reduced cellular uptake, a well-known toxicity-efficiency dilemma.[20,21] Due to the increased presence of PEG antibodies in patients, accelerated blood clearance upon re-administration occurs.[22,23] As a consequence, alternative hydrophilic polymers are investigated, for example, poly(*N*-acryloyl morpholine) (PNAM),[24,25] poly(2-oxazoline),[26,27] polysarcosine.[28,29]

To mask the positive charges of the gene carrier in the extracellular environment, the incorporation of anionic functionalities into polymeric nanocarriers has been applied to decrease the electrostatic interactions with negatively charged serum proteins.[30,31] Anionic functionalities can be integrated into the nanocarrier system either i) by electrostatic interactions forming an anionic polymer layer or ii) by incorporating anionic monomers covalently into a (block) copolymer.[31,32] The anionic polymers most commonly used for shielding are polysaccharide-, polypeptide-, or polyacrylates, such as hyaluronic acid[33,34] poly(glutamic acid),[35–37] and poly(acrylic acid), respectively.[38–41] A novel approach is represented by the (co-)assembly of different amphiphilic block copolymers containing different hydrophilic but the same hydrophobic blocks, respectively. This leads to the formation of micelles, which can potentially possess a mixed shell of cationic and neutral blocks.[42–44] Despite the potential for a wide range of functionalities and a straightforward synthesis, the study of mixed micelles containing both cationic and anionic block copolymers for gene delivery has not yet been explored. However, this approach offers a multitude of possibilities to fine-tune surface charge and charge density, thereby influencing cellular interactions and biological distribution in vivo.[45,46]

In this study, we aim to investigate whether oppositely charged mixed micelles have the potential to achieve high transfection efficiency while maintaining excellent cytocompatibility. Therefore, two sets of four diblock terpolymers were synthesized, which contained poly(*n*-butyl acrylate) (P*n*BA) as hydrophobic block and either i) a copolymerized block with hydrophilic NAM and 3-guanidinopropyl acrylamide (GPAm) or ii) NAM and 2-carboxyethyl acrylamide (CEAm). The cationic guanidinium group is known from arginine-rich cell-penetrating peptides to cause a strong interaction with anionic lipids and phosphate groups on the membrane surface.[47,48] Guanidinium-based polymers have demonstrated effective delivery of genetic material despite their pH-independent behavior in the physiological pH range ($pK_a > 12$).[49–53] A few variations of the copolymer composition and the possibility to mix the polymers at any ratio creates nearly-unlimited options to optimize the micellar structure. As a consequence, this approach offers a high chance to estimate sweet spots with ideal charge ratios and compositions for efficient transfection and high viability of the cells. However, this abundance of options also represents a challenge, as predicting effective or promising composition ranges in such a system is complex, if not impossible, due to limited knowledge of all underlying interactions. Therefore, optimizing such systems would require countless experiments, from the synthesis of the polymeric micelles to the time and resource-consuming biological investigations. In recent years, machine learning-based techniques have gained increasing popularity for a more efficient design of experiments since optimal results can be achieved with fewer experiments.[54] In particular, Gaussian process (GP) modeling has demonstrated great success due to its non-parametric nature, enabling a fast black-box optimization with very few data points. It has been proven to be an excellent tool for hyperparameter tuning in machine learning experiments, which are very cost intensive to evaluate and are an integral part of most optimizer libraries.[55] Therefore, we adapted such a process to optimize our workflow. We investigated the transfection efficiency and cytotoxicity by starting with a few micellar co-assemblies of cationic guanidinium-containing and anionic carboxyl-functionalized block copolymers. The resulting data was used to train the machine learning model in a process, which subsequently provides a next generation of compositions to be tested. The iterative process should finally identify an optimized assembly composition.

## 2. Results and Discussion

### 2.1. Synthesis and Characterization

For the preparation of mixed micelles, two sets of diblock terpolymers with a comparable overall degree of polymerization (DP) were synthesized by sequential reversible addition-fragmentation chain-transfer (RAFT) polymerization (**Table 1**). The chain transfer agent (CTA) (propanoic acid)yl butyl trithiocarbonate (PABTC) was used for the polymerization of *n*BA, generating P(*n*BA) as the first block and macroCTA (**Scheme 1**). Subsequently this first block was chain extended in a copolymerization with either i) diBoc-protected GPAm ($GPAm^{diBoc}$) and NAM or ii) *tert*-butyl-protected CEAm ($CEAm^{tB}$) and NAM to form two sets of diblock terpolymers: i) Guanidinium-functionalized P[(*n***B**A)$_x$-*b*-(**G**P$Am^{diBoc}_{y}$-*co*-**N**A$M_z$)] ($BG^{diBoc}N$) and ii) carboxy-functionalized P[(*n***B**A)$_x$-*b*-(**C**E$Am^{tB}_{y}$-*co*-**N**A$M_z$)] ($BC^{tB}N$). The two sets comprise four diblock terpolymers each with a comparable length of the hydrophobic block (DP ≈ 80) and the ionic/hydrophilic block (DP ≈ 120). The amount of GPAm and CEAm is depicted in a pie chart with the respective DP (*x*, *y*, and *z*) of each monomer (Scheme 1). For easier comparison and simplification, numbers will be used later to indicate mol% GPAm and mol% CEAm, which varied between 8 and 45 mol%. Analysis by size exclusion chromatography (SEC) revealed a monomodal, narrow molar mass distribution of $Đ = 1.09–1.12$ for the macroCTA (P(*n*BA) (Figure S4, Supporting Information). With the subsequent chain extensions, the populations shifted to higher molar masses while maintaining relatively narrow and monomodal distributions. The latter increased slightly with growing GPAm/CEAm content from 1.21 to 1.28 for $BG^{diBoc}N$ and from 1.18 to 1.22 for $BC^{tB}N$, respectively.

Furthermore, the kinetics of the copolymerization of $GPAm^{diBoc}$ and NAM were monitored by $^1$H NMR spectroscopy and SEC to estimate the distribution of the monomers in the second block. The $\ln([M]_0/[M])$ plot displayed linear pseudo-first-order polymerization kinetics for $GPAm^{diBoc}$ and NAM up

**Table 1.** Overview of the composition and characterization of the polymers used within the study and their respective GPAm and CEAm content in mol%.

| Polymer code[a)] | Composition[b)] | GPAm [mol%] | CEAm [mol%] | $M_{n,theo}$[c)] [kg mol$^{-1}$] | $M_{n,SEC}$[d)] [kg mol$^{-1}$] | $Đ$[d)] |
|---|---|---|---|---|---|---|
| P(*n*BA)$_{81}$ | – | – | – | 10.6 | 10.6 | 1.09 |
| P(*n*BA)$_{82}$ | – | – | – | 10.8 | 10.6 | 1.12 |
| BC$^{diBoc}$N-8 | P(*n*BA)$_{81}$-*b*-P(GPAm$^{diBoc}$$_{15}$-*co*-NAM$_{102}$) | 8 | – | 30.6 | 34.1 | 1.21 |
| BC$^{diBoc}$N-17 | P(*n*BA)$_{81}$-*b*-P(GPAm$^{diBoc}$$_{33}$-*co*-NAM$_{84}$) | 17 | – | 34.7 | 40.5 | 1.23 |
| BC$^{diBoc}$N-29 | P(*n*BA)$_{82}$-*b*-P(GPAm$^{diBoc}$$_{60}$-*co*-NAM$_{62}$) | 29 | – | 41.7 | 45.7 | 1.22 |
| BC$^{diBoc}$N-45 | P(*n*BA)$_{82}$-*b*-P(GPAm$^{diBoc}$$_{92}$-*co*-NAM$_{32}$) | 45 | – | 49.3 | 51.0 | 1.28 |
| BC$^{tB}$N-8 | P(*n*BA)$_{81}$-*b*-P(CEAm$^{tB}$$_{16}$-*co*-NAM$_{115}$) | – | 8 | 30.0 | 36.6 | 1.18 |
| BC$^{tB}$N-16 | P(*n*BA)$_{81}$-*b*-P(CEAm$^{tB}$$_{33}$-*co*-NAM$_{92}$) | – | 16 | 30.2 | 39.2 | 1.19 |
| BC$^{tB}$N-29 | P(*n*BA)$_{82}$-*b*-P(CEAm$^{tB}$$_{59}$-*co*-NAM$_{60}$) | – | 29 | 31.0 | 40.0 | 1.21 |
| BC$^{tB}$N-44 | P(*n*BA)$_{82}$-*b*-P(CEAm$^{tB}$$_{87}$-*co*-NAM$_{31}$) | – | 44 | 32.5 | 41.2 | 1.22 |

[a)] Numbers after hyphen represent the mol% of GPAm and CEAm; [b)] numbers were determined via $^1$H NMR spectroscopy and represent the DP of each monomer; [c)] calculated using Equation (S2), Supporting Information; [d)] determined via SEC (eluent: DMAc + 0.21% LiCl; PMMA standard).

to a reaction time of 120 min, reaching a conversion of 85% for GPAm$^{diBoc}$ and 97% for NAM (Figure S6, Supporting Information). The number-average molar mass increased linearly with the overall monomer conversion while the SEC elution traces shifted to higher molar masses, and the molar mass distribution remained narrow ($Đ$ < 1.3), indicating a controlled RAFT process. Since the plot of conversion versus time indicated that NAM is slightly more reactive compared to GPAm$^{diBoc}$ in the copolymerization, a gradient structure is expected from NAM to GPAm$^{diBoc}$ in the hydrophilic blocks (see Figure S7,

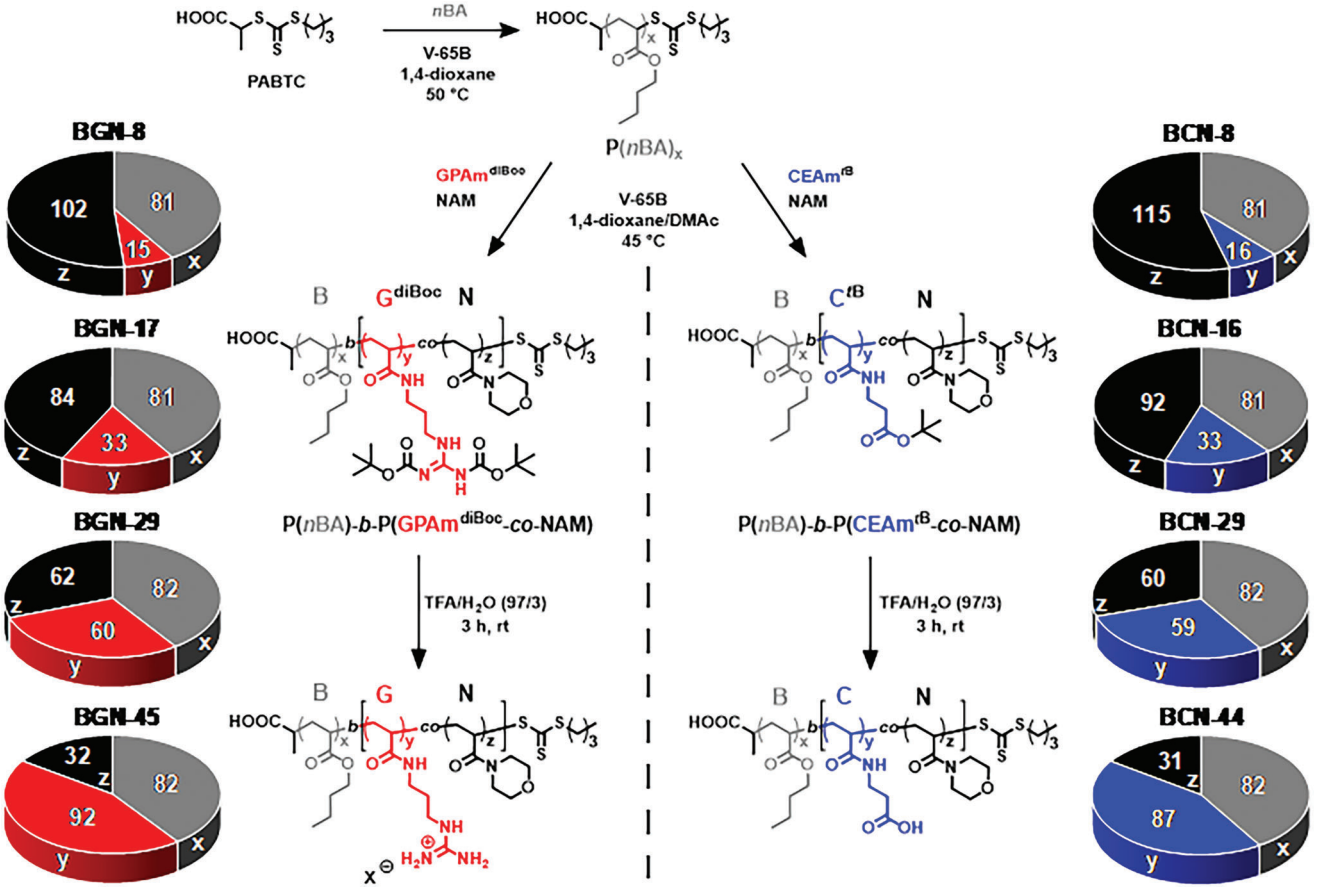


**Scheme 1.** Synthesis of the diblock terpolymers by RAFT polymerization. Compositions of BGN and BCN polymers are pictured in a pie chart with the respective DP of each monomer (grey part: DP of *n*BA (B), black part: DP of NAM (N), red part: DP of GPAm (G), blue part: DP of CEAm (C)); X$^-$: $F_3CCOO^-$.

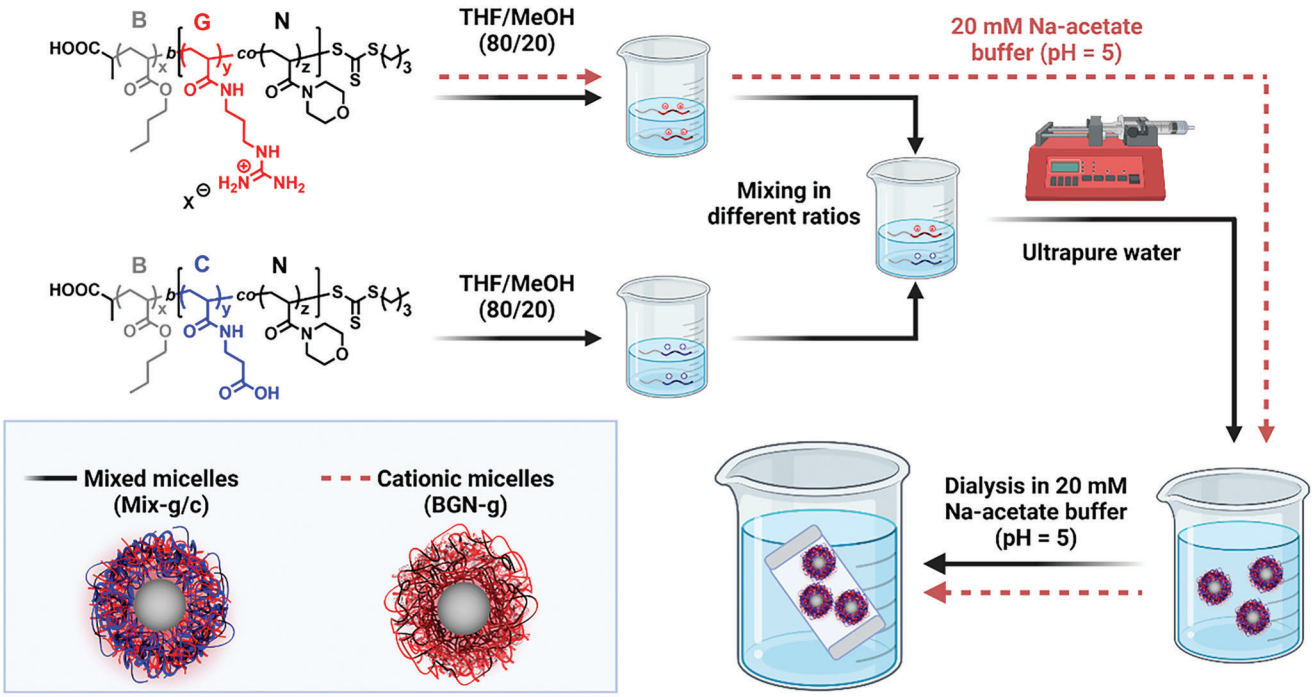


**Scheme 2.** Schematic representation of the assembly method to generate cationic micelles (dashed arrows) and mixed micelles (solid arrows) by solvent exchange: dissolving the cationic BGN and anionic BCN polymers separately in THF/MeOH, followed by mixing of both solutions in different weight percent ratios; then ultrapure water (or 20 mM NaOAc, pH = 5) was added, followed by dialysis; Mix-*g*/*c* (*g*: mol% GPAm, *c*: mol% CEAm).

Supporting Information). The kinetics of the copolymerization of CEAm$^{tB}$ and NAM were investigated similarly, indicating a controlled polymerization process (Figure S8, Supporting Information). Similar to the previous case, CEAm$^{tB}$ and NAM were converted at different rates, indicating a gradient composition from NAM to CEAm$^{tB}$ in this block (Figure S7, Supporting Information). The diblock terpolymers were finally deprotected with trifluoroacetic acid. The successful synthesis of the final polymers P[(*n***B**A)-*b*-(**G**PAm-*co*-**N**AM)] (BGN-g) and P[(*n***B**A)-*b*-(**C**EAm-*co*-**N**AM)] (BCN-c) (g: mol% GPAm, c: mol% CEAm) was confirmed by $^1$H NMR, where the peak of the Boc-/*tert*-butyl group at 1.5 ppm disappeared in both cases compared to the protected polymers (Figures S10,S11, Supporting Information).

### 2.2. Initial Micelle Assemblies and Their Characterization by Size

The micelles were assembled using a solvent exchange approach (**Scheme 2**). For the pure cationic micelles, the polymers of the BGN-diblock library were dissolved in a mixture of tetrahydrofuran/methanol (THF/MeOH 80/20 v/v%), followed by the addition of aqueous sodium acetate solution (20 mM). After dialysis against 20 mM acetate buffer, the size of the cationic micelles (BGN-g: BGN-8, BGN-17, BGN-29, and BGN-45) was investigated by dynamic light scattering (DLS), revealing intensity-weighted mean diameters (*Z*-Average value) between 23 nm and 27 nm for all different BGN-containing polymers (Table S5, Supporting Information). The micelles BGN-8 and BGN-17 displayed monomodal size distributions with polydispersity indices (PDIs) <0.2, which were stable in size for over six months (Figure S12, Supporting Information). For the assembly of the mixed micelles, the cationic BGN and anionic BCN polymers were dissolved separately in a mixture of THF/MeOH (80/20 v/v%) and subsequently mixed in different weight ratios. Then, ultrapure water was added, followed by dialysis against 20 mM sodium acetate buffer, generating mixed micelles with a common P(*n*BA) core and a mixed shell with different ratios of GPAm, CEAm, and NAM. At first, BGN-29 and BGN-45 were combined with BCN-29 and BCN-44 at different weight ratios to assemble five mixed micelles that contained a larger mol% amount of GPAm than CEAm (Mix-*g*/*c*; *g*: mol% GPAm, *c*: mol% CEAm). Details on the composition of mixed micelles can be found in Table S3, Supporting Information. An excess of the positive charge of the guanidinium group is required to guarantee the subsequent complexation of genetic material. Furthermore, it has to be kept in mind that the guanidinium group of GPAm is fully charged independently of the pH-value due to its high apparent p$K_a$ (>12),[49] while only 45% of the carboxy group of CEAm is charged at pH = 5 and 92% are charged at pH = 7 (apparent p$K_a$ ≈ 5.1).[56] DLS measurements revealed monomodal size distributions for all initially mixed micelles with an excess of Gua (Mix-19/16, Mix-25/19, Mix-27/17, Mix-19/11, Mix-30/10) with *Z*-Average values larger than the purely cationic micelles (32–68 nm) and narrow PDIs < 0.25 (Table S5, Supporting Information). Interestingly, Mix-19/16 revealed the largest *Z*-Average value (68 nm) with the smallest PDI (0.033) of all assemblies, pointing toward the formation of larger morphologies than micelles.

In addition, the mixed micelles exhibit long-term stability in solution at room temperature over nine months (Figure S13,

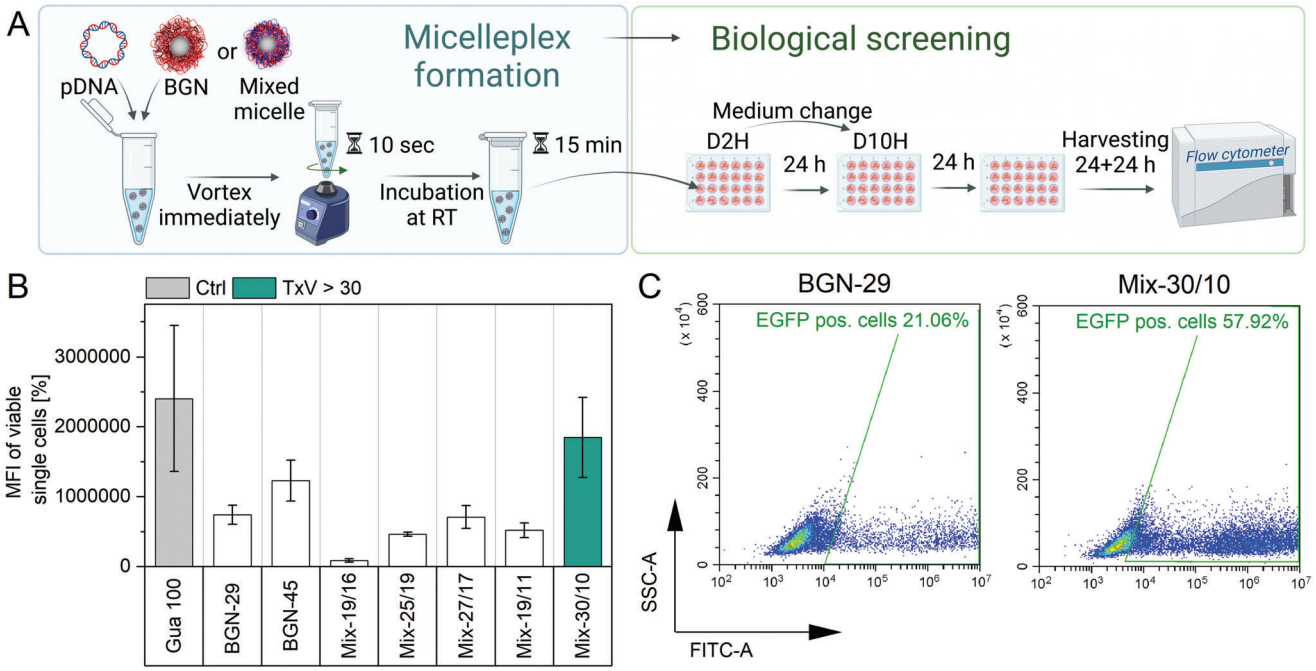


**Figure 1.** Formulation of BGN- and mixed micelles and transfection efficiency of initial 1st set of assemblies conducted via flow cytometry. A) Formulation of polyplexes/micelleplexes followed by treatment of cells at N*/P 20 and 3 µg mL$^{-1}$ of EGFP expressing pDNA in D2H for 24 h, medium change to D10H for further 24 h and measurement of transfection efficiency via flow cytometry after 24+24 h. B) Mean fluorescence intensity (MFI) value of viable single cells and cell viability measured by flow cytometry. Colored samples reveal TxV values over 30 ($n \geq 3$). C) FITC-A/SSC-dot plots of transfection efficiency of BGN-29 and Mix-30/10, determined via flow cytometry. The events within the green gate represent viable, single, EGFP-positive cells identified by gating to the negative plasmid control. The detailed gating strategy are illustrated for all samples from the 1st set exemplary from one measurement in Figure S16, Supporting Information.

Supporting Information). This is particularly encouraging considering the potential for aggregation due to the opposing charges of the cationic and anionic segments. The results indicate that the diblock terpolymers form an interpolyelectrolyte complex (IPEC) within the shell of the mixed micelles, in particular when an excess of Gua is present.[57] Only in case of Mix-30/10, a second population appeared at smaller sizes in the number- and volume-weighted size distribution after one month.

### 2.3. The 1st Set of Assemblies and Its Biological Characterization

One of the most important requirements for gene carriers is the effective complexation of the genetic material. Thus, the polymers' affinity to form a complex with the genetic material is investigated by a binding and release assay. An intercalating dye is used, whose fluorescence intensity increases upon complex formation and decreases upon displacement. Different N*/P ratios (molar ratio of protonated amines in the polymer structure to phosphates in the pDNA backbone, calculation see Supporting Information) from 3 to 20 were tested. The homopolymer $P(GPAm)_{71}$ (Gua 100), which was synthesized according to a previously described procedure, served as a control polymer.[49] It clearly revealed that the complexation affinity of the polymers was not reduced by incorporating the negatively charged CEAm diblock compared to the control Gua 100. In contrast, the mixed micelles showed a high degree of complexation with the genetic material, even at lower N*/P ratios of 3 and 5. Although the successful packaging of the genetic material is crucial, the ability of the carrier to release it at the desired location is of equal importance. Remarkably, all micelle complexes exhibited good and similar release profiles comparable with Gua 100, although the proportion of GPAm and CEAm units varied. N*/P 20 (Figure S18B, Supporting Information) was chosen as the optimal N*/P ratio for an efficient and stable complexation with good release kinetics and was, thus, used for the subsequent transfection studies. For the polyplex and micelleplex formation, an aqueous solvent method was used.[58] In this complexing process, genetic material was added to the polymer/micelle solution (**Figure 1**A) and immediately vortexed to enable polyplex/micelleplex formation. The physical-chemical characterization of the polyplexes and micelleplexes will be presented in detail in a later section.

Following this, the performance of the loaded carriers was determined in terms of transfection efficiency and cytotoxicity via flow cytometry in the human embryonic kidney cell line (HEK293T) over 24+24 h (Figure 1A). Due to the positive charge of the guanidinium group at physiological pH value and its tendency to aggregate with serum proteins, a serum-reduced medium D2H (Dulbecco's modified eagle medium (DMEM) with 2% fetal bovine serum (FBS) and 10 mM 2-[4-(2-hydroxyethyl)piperazin-1-yl]ethanesulfonic acid (HEPES) buffer to stabilize the pH value of media during transfection) was used for the incubation with pDNA containing polyplexes/micelleplexes for 24 h. Subsequently, D2H was changed to fresh full-growth medium D10H (DMEM with 10% FBS and 10 mM HEPES buffer) to supply the cells with fresh culture

medium for another 24 h (24+24 h in total) to enable good expression of enhanced GFP (EGFP). Gua 100 and the BGN-micelles, formed by BGN-polymers only, were tested as controls. To determine the transfection efficiency, the percentage of EGFP-expressing cells and the mean fluorescence intensity (MFI) of single, viable cells were analyzed via flow cytometry. The percentage of EGFP-positive cells indicates how many viable cells successfully expressed the gene. Moreover, the MFI value provides information on how effectively the gene was expressed. Thus, both values can be used to assess the effectiveness of the gene carrier. Since the focus is not only on the effectiveness but also on the cytocompatibility of the polymers, the TxV value was introduced to relate the two key parameters to each other: Transfection efficiency (EGFP-positive cells) multiplied with viability (identified via flow cytometry according to Forward Scatter (FSC)-A/Sideward Scater (SSC)-A plot). In short, our goal is to strive for a high TxV values.

Figure 1B presents the MFI, which were determined via flow cytometry of the 1st set of mixed micelles, Gua 100, and the BGN-micelles. Overall, the MFI values show the same trend and tendencies as the measured percentage of EGFP-positive cells. Therefore, only the MFI values will be shown here, and the data for EGFP-positive cells, viability and TxV values can be found in Figures S16,S17 (Supporting Information, 1st set). For the purely cationic BGN-micelles (BGN-29 and BGN-45) the one with the higher molar fraction of guanidinium exhibited higher MFI values and increased amounts of EGFP positive cells. However, the viability decreased. Increasing the percentage of GPAm units in the BGN-diblock correlated with a lower amount of NAM as shielding component. This results in increased interactions with the cell membrane, leading to increased transfection efficiency and cytotoxicity. To overcome this toxicity-efficiency dilemma, an anionic charged BCN-diblock was mixed with cationic charged BGN-diblock at a defined weight ratio to form mixed micelles. At physiological pH value, the positively charged BGN-diblock is responsible for complexing the genetic material, and the negatively charged BCN-diblock shields the excess of positive charges. By incorporating the BCN-diblock, it can be observed that a higher molar fraction of guanidinium can be introduced into the mixed micelles to achieve high transfection efficiency without a rapid increase in cytotoxicity. Thus, the advantage of incorporating the BCN-diblock is also reflected in the improvement of the TxV values. This becomes clear when comparing the mixed micelles with the BGN-diblock micelle, which have comparable GPAm units (Figure 1C)., E.g., the mixed micelles Mix-30/10 (TxV = 50) revealed four times higher TxV values than BGN-29 (TxV = 12). Hence, a clear tendency among the mixed micelles was observed: with increased positive/negative charge ratio, that is, high amount of GPAm and low amount of CEAm, the transfection efficiency increased, which led to increased TxV value. Still, the addition of negatively charged BCN-diblock was required to improve the TxV values compared to purely cationic micelles. However, it is critical to find an appropriate ratio and optimal charge balance for the combination of the two oppositely charged diblocks to achieve maximum TxV values. As this approach provides endless combinations to assemble mixed micelles, which go hand in hand with extensive laboratory screening, machine learning was applied to reduce material and temporal resources in the following assembly sets.

### 2.4. Machine Learning Approach to Optimize the Mixed Micelle Composition

The results of the above-investigated 1st set of micelles represented the basis for training a machine learning model, which was chosen to enable a more target-oriented design of the following experiments. This machine learning-driven design of experiments (ML-DoE) should help to identify the best-performing micelle compositions, using a minimum number of trials (assemblies) to save resources. Considering the nearly-unlimited possibilities, a model that predicts the formulation's outcome concerning the target parameters would be highly beneficial. Based on such a model, a hyperplane mapping of the composition parameters compared to the outcome value can be evaluated at every point, resulting in a deeper understanding of the system.

Since it is not fully understood why the combination of positive and negative charges in a polymeric nanocarrier improves the gene delivery potential, the underlying model has to be a black-box model that is usable as a universal function approximator. Classical design of experiments methods, which rely on defined functions, for example, polynomial functions, cannot be utilized. In contrast to, for example, neural networks, which usually start to become usable with thousands of data points, a Gaussian process-based model is the most reasonable choice due to the sparsity of data points in this case. Such a model works with minimal data and can be improved iteratively by adding new data points.[59] The resulting model can predict an expected outcome at every data point in the parameter space, usually in a smooth hyperplane. Furthermore, the model come with a standard deviation that can be evaluated at every point in the input parameter space, giving a metric for the uncertainty of the model, which can be used for the exploration of formulations where the model has only very little knowledge.

The micelle assembly was designed to reduce the dimensionality of the input parameter space to three dimensions: The average number of GPAm and CEAm monomers ($DP_{GPAm}$ and $DP_{CEAm}$) in the respective polymers and the weight ratio of the CEAm-bearing polymer ($ratio_{BCN}$). Since the total DP and the P*n*BA-block was comparable for all polymers, the number of NAM units in the hydrophilic/ionic block is related to the corresponding number of GPAm/CEAm units and, thus, a dependent parameter.

The optimization process has, in theory, two independent targets: High transfection efficiency (EGFP-positive cells) and viability. As a result, not a single optimum can be directly defined but a 2D Pareto-front (**Figure 2**A). Since the target of the study is to find an optimum concerning both targets, and both can be expressed as a range between 0 and 100 (0–100%), we aimed to optimize the product of both (TxV value), which approaches the maximum of 100% only if both are excellent and becomes zero as soon as one of both values gets very low. The complete parameter space can, as such, be defined as [$DP_{GPAm}$ = [0,120], $DP_{CEAm}$ = [0,120], $ratio_{BCN}$ = [0,1], TxV = [0,1]]. As can be seen in the Pearson correlation matrix (Figure 2B), the total amount of guanidinium-bearing polymer blocks (increasing proportionally with $DP_{GPAm}$ and inverse proportionally with $ratio_{BCN}$) has the highest positive correlation with the transfection efficiency, which is expected due to the positive charge, acting as a DNA carrier. At the same time, this has a negative effect on the viability, which in our

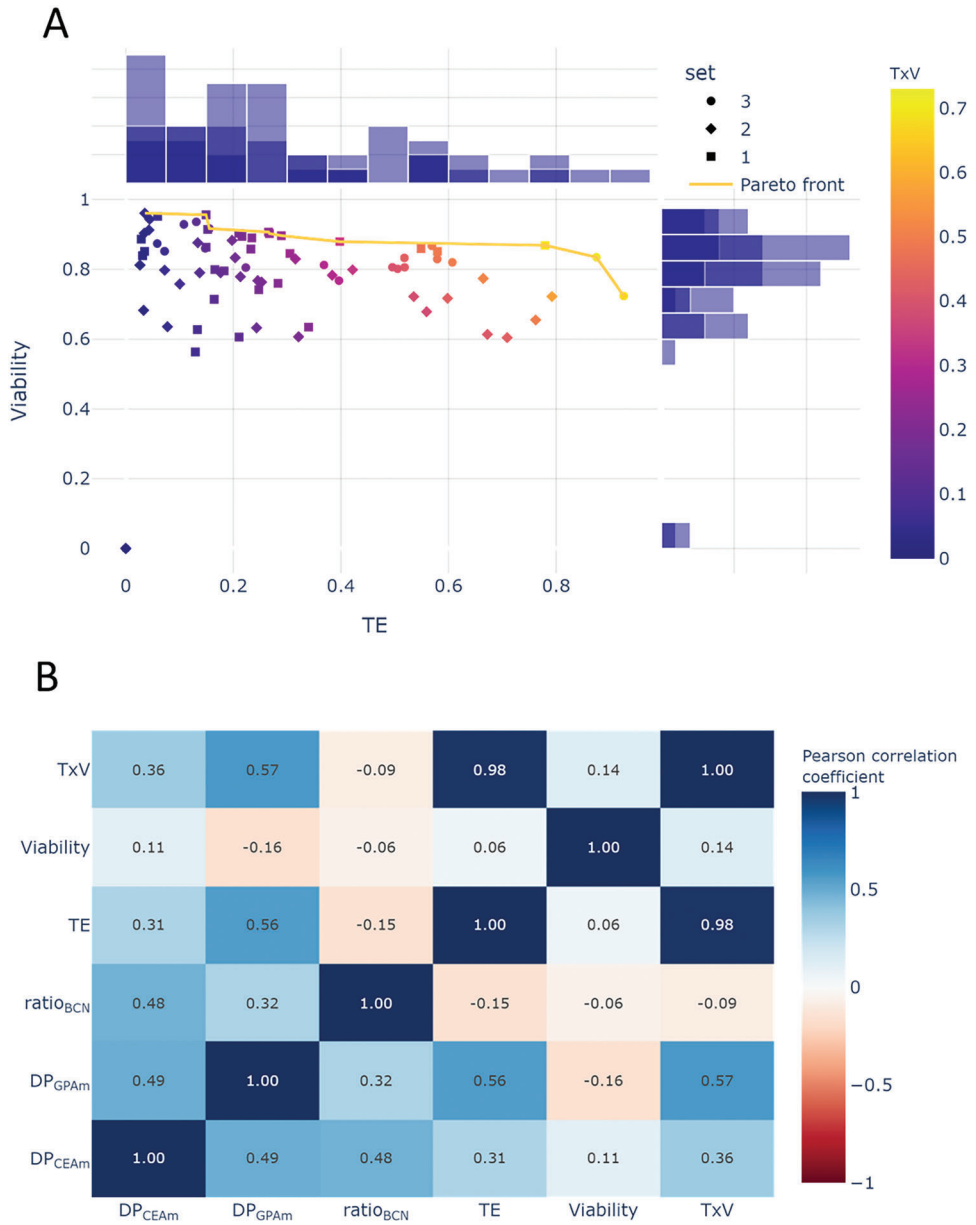


**Figure 2.** A) Visualization of the relationship between the transfection efficiency (TE) and the viability of all experimental data points and the corresponding Pareto front. As can be seen, the expected maximum viability decreases with increasing transfection efficiency and drops drastically with high efficiencies. B) In the Pearson correlation matrix, the linear influence of the parameters based on the experimental data can be estimated. The estimated linear correlation between TE and viability is low (0.06), due to the reason that most data points show a viability > 80% and drop only for high transfection efficiencies, where only a few experiments were performed, while the measured TE ranges over a much wider range of possible values. For the same reason, the correlation with TxV is much higher for the transfection efficiency compared to the correlation of TxV with viability. Furthermore, the transfection efficiency strongly correlates with the $DP_{GPAm}$, which also shows the necessity for the positive charge to act as a DNA carrier.

system should be compensated with the carboxy-bearing BCN polymers.

All input parameters are continuous, but the ratios were used as integer percentages (rounded to 1/100th) for practicality, since a finer grade would result in increasingly more experiments with diminishing returns. Furthermore, the input parameter DP was treated as a pseudo-categorical parameter since the number of available variations was limited in the given polymers. Additionally, virtual data points were introduced to the dataset to further reduce the number of experiments. Since the positive charge of the GPAm moiety is required for the complexation of the genetic material and, thus, transfection, the expected TxV-outcome of every point in the parameter space, where either the weight ratio of the BGN polymer is zero or the $DP_{GPAm}$ is zero, was set to zero. Furthermore, all available data points where the weight ratio of the CEAm-containing polymer is 1 (100% BCN) are intrinsically independent of the $DP_{GPAm}$ and can be applied along the whole $DP_{GPAm}$-input space (and vice versa). The model was trained on

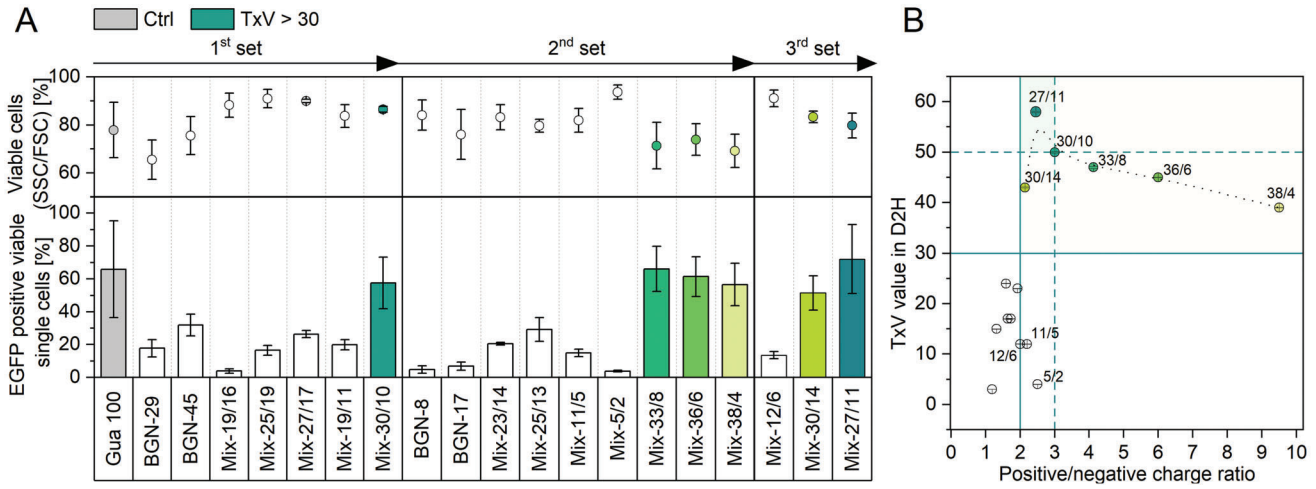


**Figure 3.** Transfection efficiency of all polyplexes/micelleplexes in D2H. A) Transfection efficiencies were investigated over 24+24 h (medium change to full growth medium after 24 h) at N*/P 20 and 3 μg $mL^{-1}$ of mEGFP-N1 pDNA on cells. Micelleplexes of 2nd and 3rd sets were inspired by a machine learning-based model. The hit candidates with a TxV value > 30 are colored. The more intense (green-blue) the color, the higher the achieved TxV values. Values represent mean ± SD ($n \geq 3$). B) Correlation between charge ratio and TxV value of transfection in D2H. Black dashed line visualizes their correlation. Green solid lines mark the boundaries of the hit micelles (yellow background with TxV > 30 and positive/negative charge ratio > 2) and dashed lines the boundaries of the best performers (green background with TxV > 50 and positive/negative charge ratio approximately between 2 and 3).

all available experimental and virtual data points during each iteration step. One of the key features of the models based on Gaussian processes is its ability to predict for the entire parameter space. Slices of the three-dimensional input space are shown in Figure S24A, Supporting Information. The ideal $ratio_{BCN}$ for the assembly is between 0.07 and 0.4, and the TxV drops very fast with a $ratio_{BCN} > 0.4$. Figure S24B, Supporting Information, shows the mean model prediction for each pseudo-categorical input combination of $DP_{GPAm}$ and $DP_{CEAm,}$ including the correlated standard deviation and the underlying data points. The model standard deviation captures the experimental deviation very well.

As mentioned, the biological results of the 1st set were included in the training data for the model, resulting in better predictive certainty and the proposal of new sample points for the following 2nd and 3rd sets. The initially proposed sample points resulted in a broader distribution in the parameter space due to the sparsity of the initial points and the correlating uncertainty in unknown regions of the parameter space (exploration phase). The model tends to propose experiments in the parameter space where no data are available to reduce the uncertainty. This exploration of the parameter space is required to prevent the model from optimizing toward a possible local maximum, as it occurs with many classical experimental optimization techniques (e.g., gradient-based).[60] The new mixed micelles after the 2nd and 3rd run are displayed in **Figure 3**A and were prepared based on suggestions of the machine learning model to reach a high TxV value. It is important to mention that the machine learning model suggested two more mixed micelle compositions (Mix-10/23 and Mix-12/21) for the 2nd set, which could not be assembled, as the micelles aggregated and precipitated during the assembly process. Since equimolar amounts or an excess of CEAm to GPAm was used in these assemblies, the aggregation could be explained by a neutral or slightly negative surface charge of the mixed micelles due to the neutralization of positive and negative charges, which destabilized the micelle structure. Successfully assembled micelles were tested for their transfection efficiency and viability in D2H.

### 2.5. Transfection and Viability of All Assemblies in Serum-Reduced Medium

Figure 3A shows the transfection efficiency (EGFP positive, single, viable cells) for all assembled micelles of the 1st, 2nd, and 3rd set. With little resource input, further five hit mixed micelles with TxV > 30 could be successfully identified. The hit rate increases after each set, which illustrates the successful training of the model by inserting experimental data values. On closer inspection, a low positive/negative charge ratio (< 2) lowered the TxV value (Figure 3B). On the other hand, increasing the positive/negative charge ratio at a specific range improved transfection efficiency and cytotoxicity. Nevertheless, a strong rise in positive/negative charge ratio (Mix-38/4) slightly increased cytotoxicity and, thus, reduced transfection efficiency. Equally important is a certain minimum content of GPAm units, which is required to form stable mixed micelles. Thus, Mix-5/2, Mix-11/5, Mix-12/6 showed lower TxV values despite positive/negative charge ratios comparable to the best performers Mix-30/10 and Mix-27/11. However, Mix-11/5 and Mix-19/11 revealed a threefold increase of the TxV value compared to their BGN micelle counterparts (BGN-8 and BGN-17, respectively). This finding confirmed improved biological performance by the incorporation of the BCN-diblock. The low transfection efficiency of Mix-19/16 compared to Mix-19/11 could be a result of the high CEAm content of the former. However, the large size of Mix-19/16 compared to the other mixed micelles could influence the biological performance as well. The results show no linear relationship between the

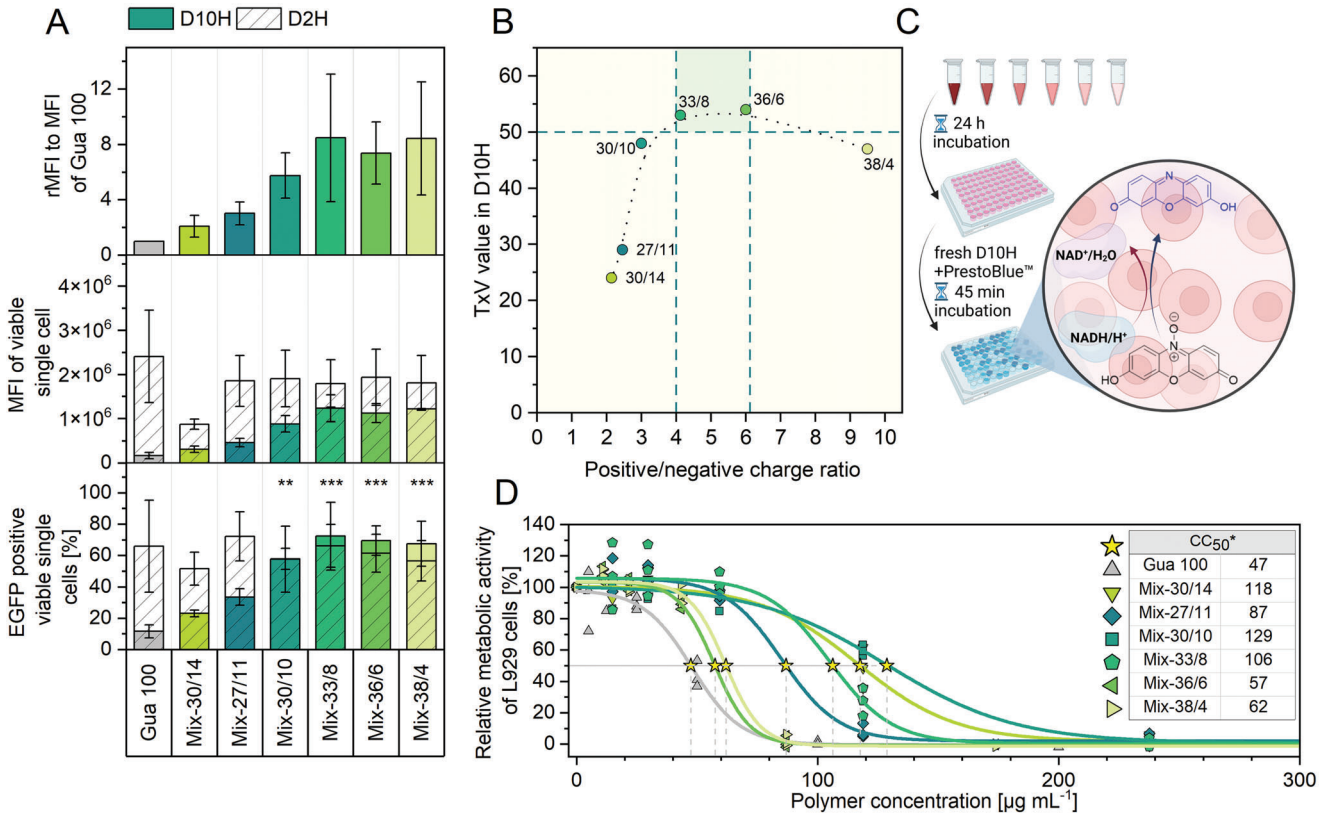


**Figure 4.** Transfection efficiency and PrestoBlue assay of Gua 100, and hit mixed micelles. A) Transfection efficiency was analyzed by flow cytometry. EGFP positive cells and mean fluorescence intensity (MFI) were investigated in D10H (colored bars) versus D2H (dashed bars) at N*/P 20, for 24+24 h. Values represent mean ± SD ($n = 3$). Statistically significant differences between respective mixed micelles and Gua 100 in D10H: $^{**}p < 0.01$, and $^{***}p < 0.001$. B) Correlation between charge ratio and TxV value of transfection in D10H. Black dashed line visualizes their correlation. Green dashed lines mark the boundaries of the best performers (green background with TxV > 50 and positive/negative charge ratio approximately between 4 and 6). C) The metabolic activity (PrestoBlue assay) in L929 cells, based on ISO10993-5, was performed with the hit mixed micelles in D10H for 24 h. D) Results of the PrestoBlue assay. Dots represent values of single repetitions, and lines were fitted with dose-response function ($n = 3$). Stars indicate polymer concentration (µg mL$^{-1}$), which induces 50% cytotoxicity.

positive/negative charge ratio and the TxV value. In contrast, an optimum charge ratio could be identified during the optimization process using machine learning (Figure 3B): Mix-30/10 and in particular Mix-27/11 with a charge ratio between 2 and 3 show TxV values of 50 and higher.

Lastly, it is crucial to mention that the guanidinium homopolymer Gua 100 achieves high TxV values in D2H. This is not astonishing and can be explained by the low serum interaction in D2H, the high charge density, and efficient endosomal release.[49]

### 2.6. Transfection in Full Growth Medium and Cytotoxicity of Optimized Mixed Micelles

The cationic homopolymer Gua 100 reached high transfection efficiencies and good TxV values in D2H. However, a more severe issue is related to the strong aggregation of such positive charged polymers with serum proteins at a physiological pH value of 7.4, resulting in low performances if transfections in full growth medium are considered.[49] Therefore, in this section, the hit mixed micelles are evaluated for their efficiency in full growth medium containing 10% FBS and 10 mM HEPES buffer (D10H) to assess whether incorporating the negative diblock into the micelles has an advantage over the guanidinium homopolymer Gua 100.

Results of the study in D10H (colored bars) are presented in **Figure 4**A in combination with previous outcomes in D2H (dashed bars) to better illustrate the influence of serum proteins. The impact of an increased proportion of serum on the transfection efficiency, in particular in the case of Gua 100, was remarkable. The percentage of EGFP-expressing cells was strongly reduced with 10% serum, and only a low protein expression (low MFI) was observed. Remarkably, all hit micelles with comparable MFI to Gua 100 in D2H, achieved double to eightfold higher MFI values than Gua 100 in D10H. Additionally, cell viability was improved as well (Figure S17B, Supporting Information). Focusing on the hit micelles, it is worth mentioning that the mixed micelles revealed significantly more EGFP positive cells in D10H than Gua 100. Similarly to D2H, an optimal GPAm content can be also found in D10H, which is needed to balance the interaction with serum and cell transfection. In particular, Mix-33/8 and Mix-36/6 with a positive/negative charge ratio between 4 and 6 were identified as best performing mixed micelles in D10H with a TxV > 50 (Figure 4B). Interestingly,

the best performer in D2H is not identical to that in D10H. Moreover, mixed micelles with a rather high charge ratio performed better in D10H. However, cytotoxicity likewise increased with higher charge ratios. This result is in agreement with a study that found poly(amido amine) copolymers with 80 mol% of the guanidinium and 20 mol% of the carboxy group (positive/negative charge ratio of 4) to have the optimal ratio to achieve high transfection efficiency.[53] However, the gene expression was 30% reduced in 10% serum-containing medium, indicating that combining positive and negative charges in a copolymer structure might not reduce or compensate interactions with serum proteins on the same level as the mixed micelle composition in our study. The lower MFI in D10H compared to D2H, which correlates with the amount of expressed EGFP, indicated that some micelleplexes were quantitatively removed from the system due to the interactions with serum proteins. This could explain why a higher positive/negative charge ratio is needed for successful transfection in the D10H in comparison to D2H.

To further elucidate the cytocompatibility of the hit mixed micelles in comparison to Gua 100 homopolymer, a PrestoBlue assay in the adherent type of mouse fibroblast cell line (L929), based on ISO10993-5, was performed (Figure 4C), and the $CC_{50}$ (critical concentration at 50% viability) was determined (Figure 4D). All incubations with mixed micelles revealed increased cell viability compared to the cationic homopolymer Gua 100. Accordingly, reducing CEAm content, which is related to an increased positive net charge, leads to reduced cytocompatibility of the mixed micelles.

The cytocompatibility was further investigated via hemolysis and aggregation assays to study the impact of the mixed micelles on the cell membrane of erythrocytes in the absence of serum proteins (Figure S19A, Supporting Information). In comparison to Gua 100, all tested mixed micelles led to similar aggregation, but stronger hemolysis of erythrocytes at high concentrations (Figure S19C,D, Supporting Information). The influence of the negatively charged CEAm content in mixed micelles on hemolysis but not on aggregation is interesting. This leads to the assumption that charge compensation by GPAm and CEAm units creates a non-charged environment, which results in strong membrane interaction and higher hemolysis.

In general, in full growth medium, the toxicity-efficiency dilemma of cationic polymers seems to be overcome by incorporating anionic polymers into the mixed micelle composition. This is clearly demonstrated by the increase in the TxV value from 9 of the homopolymer to 54 of the best performing mixed micelles. Furthermore, the presence of serum provokes a stronger influence of the positive-negative charge ratio on efficiency than serum-reduced conditions. A molar ratio of >30% GPAm and a positive/negative charge ratio between ≈ 2 and 3 in D2H and a higher positive/negative charge ratio between ≈ 4 and 6 in D10H appear to be the optimal window for achieving a good balance between efficient transfection and high cytocompatibility with TxV ≥ 50. The strong hemolysis of the mixed micelles is crucial for the successful transfection in full growth medium. The higher surplus of positive charge in D10H is necessary to balance the remaining serum interactions and the effective membrane interactions. In summary, the results emphasize that an ideal charge ratio (GPAm and CEAm units) is one successful method to maintain optimal membrane interactions to trigger internalization of the micelleplexes without adversely affecting cell viability in presence of serum.

### 2.7. Stability and Size of Mixed Micelles and Micelleplexes

Since particle size and surface charge influence particle uptake and relate to its transfection efficiency, it is crucial to verify the size and surface charge of the micelles and corresponding micelleplexes. Particles with sizes below 200 nm are favored for controlled endocytosis and prolonged blood circulation. An optimal amount of cationic charge is required for cellular uptake and intracellular distribution and, thus, high efficiency.[56] Therefore, the hit mixed micelles and their micelleplexes were characterized by DLS measurements and compared to the Gua 100 homopolymer. Overall, the hit mixed micelles reveal a hydrodynamic size below 40 nm (31–38 nm) with a PDI ≤ 0.3 (**Figure 5**A). All hit micelles, except Mix-36/6 and Mix-38/4, showed unimodal size distributions (Figures S13–S15, Supporting Information). With pDNA complexation, an increase in size compared to the pure mixed micelles was observed, but the overall sizes of the micelleplexes remain below 100 nm (75–85 nm), showing unimodal size distributions with PDIs below 0.3 (Figure S20, Supporting Information). One of the best performing micelleplexes (Mix-33/8) was further investigated by cryo-TEM (Figure 5B). The cryo-TEM images revealed chains of micelleplexes, which tended to arrange in loose clusters but did not coagulate fully, which is most likely related to their still positive surface charge (Figure S21A, Supporting Information). On some occasions, the so-called "beads-on-a-string" packing motif is observed, where micelles are connected in strands and participate in the complexation of one or a few DNA strands.[16] This packing structure could lead to an advantage for micelleplexes compared to polyplexes regarding gene expression. The complexation is not as dense as in a polyplex, but it is stable enough to allow successful gene transfer and expression.[16] In addition, the size of the individual Mix-33/8-micelleplex determined by cryo-TEM is 49 nm, which is smaller than the intensity-weighted hydrodynamic size measured by DLS (79 nm) due to overrepresentation of larger particles according to the Rayleigh equation.[61]

## 3. Conclusion

Genetic material has become an indispensable active ingredient in nanomedicine. Due to its propensity to degrade and circumvent its immune-activating potential, a carrier is required. An ideal carrier enables stable packaging, protection for safe transportation to the site of action, and exhibits high efficiency and cytocompatibility. Among others, cationic polymers represent a promising platform, offering the advantage of the chemical variety and synthetic versatility with clearly defined structure and composition. In our studies, we focus on polymeric micelles and optimizing their composition, especially by introducing anionic functionalities, to meet the requirements of an ideal genetic carrier. A library of well-defined guanidinium- and carboxy-based diblock terpolymers with a comparable length of the hydrophobic (P*n*BA) and hydrophilic/ionic segment was successfully synthesized. The diblock terpolymers contained either the positively

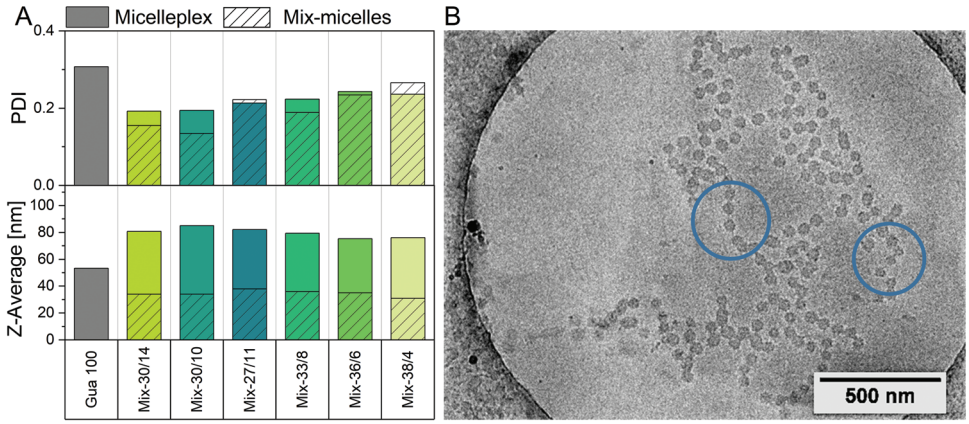


**Figure 5.** A) DLS measurement of best-performing mixed micelles revealed an average size below 40 nm and a small PDI < 0.3; DLS measurement of micelleplexes revealed an average size below 100 nm and a small PDI < 0.3. B) Cryo-TEM image of Mix-33/8-micelleplexes. Blue circles highlight the areas where the "beads-on-a-string" motif is visible.

charged guanidinium-functional monomer GPAm or the negatively charged carboxy-functional CEAm in combination with the hydrophilic NAM. The positive charge serves to complex the genetic material and the negative charge should effectively balance the excess of positive charges, which is responsible for high cytotoxicity. Therefore, the GPAm- and CEAm-based polymers (BGN-diblock and BCN-diblock) were assembled into mixed micelles with varying mol% content of the positively charged guanidinium group and negatively charged carboxy group. First, assembled micelles were tested for their ability to complex and release genetic material. The results revealed only little to no effect on complexation ability or release kinetic despite inserting negative diblocks. Transfection efficiency and viability in serum-reduced medium (D2H) were analyzed via flow cytometry and the TxV value was introduced to correlate these two main targets. With the 1st set of mixed micelles, one promising candidate with TxV > 30 could be identified. Since this method provided countless combination opportunities, a machine learning-based model was applied to save resources. A Gaussian process-based model has been used successfully to target high TxV values because it can work with minimal data and can be trained iteratively by adding new data points. Since it was not fully understood how the combination of positive and negative charges in a polymeric nanocarrier increased the potential for gene delivery, a black box model was applied to effectively ascertain the best scope of positive/negative charge ratios for effective transfection and high viability by using the input parameters: DP of GPAm and CEAm units, weight ratio of the CEAm-bearing polymer ($ratio_{BCN}$).

With only two runs, a narrow window with optimal charge ratios for the mixed micelles was identified in D2H for further five hit mixed micelles with TxV values > 30. A mol percentage above 30% GPAm was identified as effective in our approach for the investigated conditions in serum-reduced medium (D2H). Within this scope, we identified further an optimal positive/negative charge ratio (mol% of GPAm / mol% of CEAm) between 2 and 3, where the positive charge excess was adequately, yet not fully compensated, and a TxV value above 50 was achieved. Beyond this ratio, the toxicity increased and the TxV value decreased.

To prove the superiority of the mixed micelles, the hit micelles were further investigated in full growth medium (D10H). While the guanidinium homopolymer reached high transfection efficiencies in D2H but not D10H, the mixed micelles outperformed the control polymer in D10H. The MFI of the best-performer, Mix-33/8 (70% EGFP positive cells), was eightfold higher, and the TxV value (53) was fivefold higher than the Gua 100 homopolymer. This indicated a significant impact of the negatively charged CEAm-diblock on the performance of the mixed micelles. Interestingly, in D10H, a higher excess of positively charge GPAm units was needed to achieve TxV > 50 in comparison to D2H. This emphasizes that not only sufficient CEAm units are crucial, but that a defined proportion of GPAm is indispensable for complexation of the genetic material, for suitable membrane interaction, for effective transfection and to maintain cytocompatibility.

In conclusion, machine learning was successfully applied to predict the optimal window of positive/negative charge ratio and best compositions of mixed micelles based on oppositely charged block copolymers to avoid strong serum interactions and trigger internalization, retaining cell membrane integrity and viability while still achieving high transfection efficiency. The results underline that incorporating anionic functionalities into polymeric micelles is a successful strategy to optimize their properties as an effective nanocarrier.

## 4. Experimental Section

The experimental section can be found in the Supporting information.

## Supporting Information

Supporting Information is available from the Wiley Online Library or from the author.

## Acknowledgements

K.L., L.S.R., and J.K. contributed equally to this work. This work was supported by the Bundesministerium für Bildung und Forschung (BMBF, Germany, #13XP5034A PolyBioMik) and by the DFG-funded Collaborative Research Center PolyTarget (SFB 1278, projects B01, C06 and Z01, project ID: 316213987). The authors further acknowledge support of this work by

 

the "Thüringer Aufbaubank (TAB)" (2021 FGI 0005) and the "Europäischer Fond für regionale Entwicklung (EFRE)" (2018FGI0025) for funding of flow cytometry devices at the JCSM. J.C.B. also thanks the German Research Foundation (DFG) for generous funding within the Emmy-Noether Programme (Project-ID: 358263073). The authors gratefully acknowledge Dr. Grit Festag for maintaining the SEC facilities. The authors gratefully acknowledge Sandra Henk, Elisabeth Preußger, Carolin Kellner, and Bärbel Beringer-Siemers for taking splendid care of the cell lines and pDNA preparation. Furthermore, the authors gratefully acknowledge Elisabeth Moek for assistance in transfection assays. The authors gratefully acknowledge Dr. Liam Martin for his support at the beginning of this research. The graphic for the Table of Contents was created with BioRender.com.

Open access funding enabled and organized by Projekt DEAL.

## Conflict of Interest

The authors declare no conflict of interest.

## Data Availability Statement

The data that support the findings of this study are available from the corresponding author upon reasonable request.

## Keywords

block copolymers, design of experiment, gene delivery, guanidinium, machine learning, micelles

Received: July 20, 2023
Revised: September 4, 2023
Published online: October 4, 2023

[1] L. Schoenmaker, D. Witzigmann, J. A. Kulkarni, R. Verbeke, G. Kersten, W. Jiskoot, D. J. A. Crommelin, *Int. J. Pharm.* **2021**, *601*, 120586.
[2] L. Yang, L. Gong, P. Wang, X. Zhao, F. Zhao, Z. Zhang, Y. Li, W. Huang, *Pharmaceutics* **2022**, *14*, 2682.
[3] H. Yin, R. L. Kanasty, A. A. Eltoukhy, A. J. Vegas, J. R. Dorkin, D. G. Anderson, *Nat. Rev. Genet.* **2014**, *15*, 541.
[4] H. Zu, D. Gao, *AAPS J.* **2021**, *23*, 78.
[5] R. Kumar, C. F. Santa Chalarca, M. R. Bockman, C. V. Bruggen, C. J. Grimme, R. J. Dalal, M. G. Hanson, J. K. Hexum, T. M. Reineke, *Chem. Rev.* **2021**, *121*, 11527.
[6] A. C. Rinkenauer, S. Schubert, A. Traeger, U. S. Schubert, *J. Mater. Chem. B* **2015**, *3*, 7477.
[7] A. Aied, U. Greiser, A. Pandit, W. Wang, *Drug Discovery Today* **2013**, *18*, 1090.
[8] I. Jarak, M. Pereira-Silva, A. C. Santos, F. Veiga, H. Cabral, A. Figueiras, *Appl. Mater. Today* **2021**, *25*, 101217.
[9] H. Cabral, K. Miyata, K. Osada, K. Kataoka, *Chem. Rev.* **2018**, *118*, 6844.
[10] M. G. Hanson, C. J. Grimme, C. F. Santa Chalarca, T. M. Reineke, *Bioconjugate Chem.* **2022**, *33*, 2121.
[11] M. Y. Marzbali, A. Y. Khosroushahi, *Cancer Chemother. Pharmacol.* **2017**, *79*, 637.
[12] Y. Mai, A. Eisenberg, *Chem. Soc. Rev.* **2012**, *41*, 5969.
[13] T. H. Epps, III, R. K. O'reilly, *Chem. Sci.* **2016**, *7*, 1674.
[14] M. Pereira-Silva, I. Jarak, A. C. Santos, F. Veiga, A. Figueiras, *Eur. J. Pharm. Sci.* **2020**, *153*, 105461.
[15] Y. Jiang, T. M. Reineke, T. P. Lodge, *Macromolecules* **2018**, *51*, 1150.
[16] Z. Tan, Y. Jiang, W. Zhang, L. Karls, T. P. Lodge, T. M. Reineke, *J. Am. Chem. Soc.* **2019**, *141*, 15804.
[17] H. Wang, S. Ding, Z. Zhang, L. Wang, Y. You, *J. Gene Med.* **2019**, *21*, e3101.
[18] C.-M. J. Hu, R. H. Fang, B. T. Luk, L. Zhang, *Nanoscale* **2014**, *6*, 65.
[19] S. Schöttler, K. Landfester, V. Mailänder, *Angew. Chem., Int. Ed.* **2016**, *55*, 8806.
[20] Y. Fang, J. Xue, S. Gao, A. Lu, D. Yang, H. Jiang, Y. He, K. Shi, *Drug Delivery* **2017**, *24*, 22.
[21] Y. Zhang, A. Satterlee, L. Huang, *Mol. Ther.* **2012**, *20*, 1298.
[22] T. Ishihara, T. Maeda, H. Sakamoto, N. Takasaki, M. Shigyo, T. Ishida, H. Kiwada, Y. Mizushima, T. Mizushima, *Biomacromolecules* **2010**, *11*, 2700.
[23] A. S. A. Lila, H. Kiwada, T. Ishida, *J. Controlled Release* **2013**, *172*, 38.
[24] X. Yao, C. Qi, C. Sun, F. Huo, X. Jiang, *Nano Today* **2023**, *48*, 101738.
[25] P. H. Kierstead, H. Okochi, V. J. Venditto, T. C. Chuong, S. Kivimae, J. M. J. Fréchet, F. C. Szoka, *J. Controlled Release* **2015**, *213*, 1.
[26] H. Bludau, A. E. Czapar, A. S. Pitek, S. Shukla, R. Jordan, N. F. Steinmetz, *Eur. Polym. J.* **2017**, *88*, 679.
[27] M. Grube, M. N. Leiske, U. S. Schubert, I. Nischang, *Macromolecules* **2018**, *51*, 1905.
[28] Y. Hu, Y. Hou, H. Wang, H. Lu, *Bioconjugate Chem.* **2018**, *29*, 2232.
[29] S. S. Nogueira, A. Schlegel, K. Maxeiner, B. Weber, M. Barz, M. A. Schroer, C. E. Blanchet, D. I. Svergun, S. Ramishetti, D. Peer, P. Langguth, U. Sahin, H. Haas, *ACS Appl. Nano Mater.* **2020**, *3*, 10634.
[30] A. Bernkop-Schnurch, *Adv. Drug Delivery Rev.* **2018**, *62*, 136.
[31] Y. Hattori, *J. Genet. Med. Gene Ther.* **2017**, *1*, 003.
[32] K. Dutta, R. Das, J. Medeiros, P. Kanjilal, S. Thayumanavan, *Adv. Funct. Mater.* **2021**, *31*, 2011103.
[33] M. He, Y. Wang, X. Chen, Y. Zhao, K. Lou, Y. Wang, L. Huang, X. Hou, J. Xu, X. Cai, Y. Cheng, M. Lan, Y. Yang, F. Gao, *J. Controlled Release* **2020**, *319*, 1.
[34] K. Liang, K. H. Bae, F. Lee, K. Xu, J. E. Chung, S. J. Gao, M. Kurisawa, *J. Controlled Release* **2016**, *226*, 205.
[35] J. Ma, J. Zhang, L. Chi, C. Liu, Y. Li, H. Tian, *Chin. Chem. Lett.* **2020**, *31*, 1427.
[36] T. Kurosaki, M. Uematsu, K. Shimoda, K. Suzuma, M. Nakai, T. Nakamura, T. Kitahara, T. Kitaoka, H. Sasaki, *Biol. Pharm. Bull.* **2013**, *36*, 96.
[37] E. Hamada, T. Kurosaki, J. Hashizume, H. Harasawa, H. Nakagawa, T. Nakamura, Y. Kodama, H. Sasaki, *Pharmaceutics* **2021**, *13*, 126.
[38] F. Richter, K. Leer, L. Martin, P. Mapfumo, J. I. Solomun, M. T. Kuchenbrod, S. Hoeppener, J. C. Brendel, A. Traeger, *J. Nanobiotechnol.* **2021**, *19*, 292.
[39] S. K. Tripathi, Z. Ahmadi, K. C. Gupta, P. Kumar, *Colloids Surf., B* **2016**, *140*, 117.
[40] S. Wang, *Front. Chem.* **2021**, *9*, 645297.
[41] A. J. Convertine, D. S. W. Benoit, C. L. Duvall, A. S. Hoffman, P. S. Stayton, *J. Controlled Release* **2009**, *133*, 221.
[42] Q. Li, X. Hao, J. Lv, X. Ren, K. Zhang, I. Ullah, Y. Feng, C. Shi, W. Zhang, *J. Mater. Chem. B* **2017**, *5*, 1673.
[43] M. O. Pujol, D. J. L. Coleman, C. D. Allen, O. Heidenreich, D. A. Fulton, *J. Controlled Release* **2013**, *172*, 939.
[44] M. Miteva, K. C. Kirkbride, K. V. Kilchrist, T. A. Werfel, H. Li, C. E. Nelson, M. K. Gupta, T. D. Giorgio, C. L. Duvall, *Biomaterials* **2015**, *38*, 97.
[45] M. J. Barthel, A. C. Rinkenauer, M. Wagner, U. Mansfeld, S. Hoeppener, J. A. Czaplewska, M. Gottschaldt, A. Träger, F. H. Schacher, U. S. Schubert, *Biomacromolecules* **2014**, *15*, 2426.
[46] A. T. Press, A. Ramoji, M. Vd Lühe, A. C. Rinkenauer, J. Hoff, M. Butans, C. Rössel, C. Pietsch, U. Neugebauer, F. H. Schacher, M. Bauer, *NPG Asia Mater.* **2017**, *9*, e444.
[47] S. Futaki, I. Nakase, *Acc. Chem. Res.* **2017**, *50*, 2449.

 

[48] G. Gasparini, E.-K. Bang, J. Montenegro, S. Matile, *Chem. Commun.* **2015**, *51*, 10389.
[49] F. Richter, L. Martin, K. Leer, E. Moek, F. Hausig, J. C. Brendel, A. Traeger, *J. Mater. Chem. B* **2020**, *8*, 5026.
[50] Y. Zhou, S. Han, Z. Liang, M. Zhao, G. Liu, J. Wu, *J. Mater. Chem. B* **2020**, *8*, 5564.
[51] F. J. Hack, C. Cokca, S. Städter, J. Hülsmann, K. Peneva, D. Fischer, *Macromol. Rapid Commun.* **2021**, *42*, e2000580.
[52] L. Martin, R. Peltier, A. Kuroki, J. S. Town, S. Perrier, *Biomacromolecules* **2018**, *19*, 3190.
[53] Y. Sun, H. Liu, T. Yang, L. Lang, L. Cheng, H. Xing, L. Yang, P. Ding, *Colloids Surf., B* **2019**, *175*, 10.
[54] A. Hasanzadeh, M. R. Hamblin, J. Kiani, H. Noori, J. M. Hardie, M. Karimi, H. Shafiee, *Nano Today* **2022**, *47*, 101665.
[55] S. Shekhar, A. Bansode, A. Salim, in *2021 IEEE Asia-Pacific Conf. on Computer Science and Data Engineering (CSDE)*, IEEE, Piscataway, NJ **2021**, p. 1.
[56] J. I. Solomun, L. Martin, P. Mapfumo, E. Moek, E. Amro, F. Becker, S. Tuempel, S. Hoeppener, K. L. Rudolph, A. Traeger, *J. Nanobiotechnol.* **2022**, *20*, 336.
[57] D. V. Pergushov, A. H. E. Müller, F. H. Schacher, *Chem. Soc. Rev.* **2012**, *41*, 6888.
[58] J. I. Solomun, G. Cinar, P. Mapfumo, F. Richter, E. Moek, F. Hausig, L. Martin, S. Hoeppener, I. Nischang, A. Traeger, *Int. J. Pharm.* **2021**, *593*, 120080.
[59] S. Myren, E. Lawrence, *Stat. Anal. Data Min.* **2021**, *14*, 606.
[60] L. Sun, L. J. Hong, Z. Hu, *Oper. Res.* **2014**, *62*, 1416.
[61] M. D. Lechner, *J. Serb. Chem. Soc.* **2005**, *70*, 361.

 